BER the international journal of bridge engineering management and research

Key Limit States of Cable-Supported Bridges for Structural Robustness Evaluation

Qian Chen[1,*]; Hongfan Wang[2]; Anil K. Agrawal[3]; Sherif El-Tawil[4]; Baidurya Bhattacharya[5] and Waider Wong[6]

Submitted: 10 August 2025 **Accepted:** 08 October 2025 **Publication date:** 10 January 2026

DOI: 10.70465/ber.v3i1.52

Abstract: Cable-supported bridges, such as suspension bridges, cable-stayed bridges, and tied-arch bridges, play important roles in the transportation infrastructure systems. Failure of these bridges can lead to heavy casualties and significant economic losses. However, the resistance to system-level failure under specified member-loss scenario(s), also called structural robustness, of these types of bridges and the key limit states for structural evaluation have not been adequately studied. In this paper, push-down analysis is presented as a method to identify the key limit states of cable-supported bridges for structural robustness evaluation. The above analysis was conducted in LS-DYNA® on three disparate long-span cable-supported bridges, that is, a suspension bridge, a cable-stayed bridge, and a tied-arch bridge. The failure of key structural components of the bridges was monitored closely during push-down analyses, and several key limit states were identified. Bridges with single-member loss were also pushed down, and their responses were compared to the behavior of the corresponding intact bridges to evaluate the effect of member loss on push-down capacity in the context of the identified limit states. The results show that the three mentioned cable-supported bridges exhibit similar bilinear load–displacement curves during push-down analysis. Comparison of the overall performance of the identified key limit states indicates high capacity for the design live loads. The overall performance is affected negatively by cable loss, and the effects vary depending on the location of the cable loss and the pattern of live-load distribution. Despite these adverse effects, the capacities of the identified key limit states for these bridges under damaged scenarios are not reduced significantly.

Author keywords: Cable-supported bridges; member loss; push-down analysis; structural robustness; key limit states

Introduction

Cable-supported bridges, such as suspension bridges, cable-stayed bridges, and tied-arch bridges, are widely used around the world. They usually play important roles in the transportation infrastructure systems. However, failures of these types of bridges have been observed in the past. The Kutai Kartanegara Bridge, a suspension bridge, collapsed on November 26, 2011, resulting in at least 20 fatalities.[1] Morandi's Polcevera Viaduct, a cable-stayed bridge, collapsed on August 14, 2018, leading to 43 deaths.[2] The Nanfang'ao Bridge, a tied-arch bridge, collapsed on October 1, 2019, causing 6 deaths.[3] The failures of these bridges resulted in not only heavy casualties but also significant economic losses. Hence, it is important to ensure the structural robustness, the resistance to system-level failure under different initiated member-loss scenario(s), of cable-support bridges. Moreover, understanding the key limit states (LSs) of these bridges is crucial to maintaining their structural integrity and robustness.

Some investigators have investigated structural robustness in terms of load capacity-based measures. Frangopol and Curley[4] proposed a deterministic indicator in terms of the reserve strength of the damaged and intact structures and applied it to two simple truss examples subjected to different damage scenarios. In a series of NCHRP research studies,[5–7] three load factors were used to quantify the structural redundancy of typical short-to-medium-span bridges. These factors correspond to the LSs of first-member failure, ultimate capacity, and damage condition. Robustness of a simple structural system was evaluated by Maes et al.[8] through residual system strength. Wisniewski et al.[9] evaluated the robustness and overall system capacity of a set of existing railway bridges. Izzuddin et al.[10] measured the structural robustness of multistory buildings due to sudden column loss by system pseudo-static capacity. The robustness of building systems was investigated by Khandelwal and

*Corresponding Author: Qian Chen.
Email: chenqian022@hotmail.com
[1]Ph.D, Department of Civil and Environmental Engineering, The City College of New York, New York, NY 10031
[2]Postdoctoral Researcher, Department of Civil and Environmental Engineering, The City College of New York, New York, NY 10031
[3]Professor, Department of Civil and Environmental Engineering, The City College of New York, New York, NY 10031
[4]Professor, Department of Civil and Environmental Engineering, University of Michigan, Ann Arbor, MI 48109
[5]Professor, Department of Civil Engineering, Indian Institute of Technology Kharagpur, WB 721302, India
[6]Engineer, Federal Highway Administration, Baltimore, MD 21201

Discussion period open till six months from the publication date. Please submit separate discussion for each individual paper. This paper is a part of the Vol. 3 of the International Journal of Bridge Engineering, Management and Research (© BER), ISSN 3065-0569.

El-Tawil[11] in terms of overload factor under different push-down methods. Shoghijavan and Starossek[12] evaluated the robustness of cable-supported bridges using a simplified parallel load-bearing system. However, only the stress increase ratio of the cable adjacent to the failed cable in a cable-loss scenario was investigated.

The abovementioned research mainly focused on buildings, short-to-medium-span bridges, or simplified models for long-span cable-supported bridges. Chen et al.[13] proposed a reliability-based framework, which was designed to evaluate the structural robustness of short-, medium-, and long-span cable-supported bridges. The proposed approach notably enables the evaluation of structural robustness for user-specified LSs on a common and unified basis, and it was applied to different examples of long-span cable-supported bridges. However, due to the length constraints of that publication, this paper discusses the rationale behind the selection of the key LSs and the common characteristics among them across different long-span cable-supported bridges.

In this paper, push-down analysis is presented as a method to identify the key LSs of cable-supported bridges for structural robustness evaluation. During the push-down analyses, the failure of key structural components was closely monitored, leading to the identification of several key LSs. Furthermore, this study compared the responses of bridges subjected to push-down analysis after the loss of a single member with the behavior of the corresponding intact bridges. This comparison was made to assess the impact of member loss on push-down capacity concerning the identified key LSs. The above analysis was conducted in LS-DYNA®[14] on three disparate long-span cable-supported bridges, that is, a suspension bridge, a cable-stayed bridge, and a tied-arch bridge, as shown in Fig. 1. The explicit finite element (FE) analysis capabilities provided by LS-DYNA® are preferable when dealing with scenarios that entail highly nonlinear material behavior, large deformations, contact, and rapid load application associated with sudden member loss.

The simulation process of push-down analysis mainly includes two steps: (1) applying dead loads (DLs) and live loads (LLs) on the bridges (intact bridges or damaged bridges with single-member loss) and (2) pushing the bridges down with an incrementally increasing LL, which was proportionally scaled during the analysis. Further details can be found in Agrawal et al.[15]. In this study, only single-member-loss cases (loss of one suspender, stay cable, or hanger) were considered, as these represent the most common damage scenarios considered in the design guidelines for cable-supported bridges. For example, PTI[16] requires that all cable-stayed bridges shall be capable of withstanding the loss of any cable without the occurrence of structural instability. Nevertheless, the proposed push-down framework is readily extendable to other types of failures, including progressive multimember failures.

Suspension Bridge

As shown in Fig. 1a, a three-span suspension bridge was selected as the first prototype bridge. The prototype bridge was designed in accordance with the 1961 AASHO Specifications.[17] It consists of a 655.32-m center span and two 228.60-m side spans. The two steel towers are 127.43 m high. The sag ratio of the main cables at the center span is 1:10. The longitudinal stiffening truss girders are supported by 69 pairs of suspenders, and each suspender consists of four steel ropes. There are two types of suspenders: (i) Type I—made of steel ropes with a diameter of 58.74 mm and (ii) Type II—made of steel ropes with a diameter of 63.50 mm. Eleven pairs of suspenders at the middle of the center span are Type II, and the other suspenders are Type I. The suspender spacing is 15.81 m in the center span and 15.37 m in the side spans. The suspender IDs increase from left to right (Fig. 2). The FE model of the suspension bridge developed in LS-DYNA® is shown in Fig. 3. The design uniform LL for the prototype suspension bridge was 32.836 kN/m. Three LL distributions were presented in this paper: (1) LL1—uniform LL applied on all three spans; (2) LL2—uniform LL applied on the two side spans only; and (3) LL3—uniform LL applied on the center span only. The details about the model's construction, calibration and validation, material nonlinearity consideration, LL application, and member removal simulation process can be found in Wang et al.[18,19].

Analysis results of intact bridge

Push-down analyses of the intact bridge (PDI) were first conducted under the three live-load distributions, that is, LL1–LL3, and they are denoted by PDI1, PDI2, and PDI3, respectively. With the increasing LL, both axial forces in the main cables and bridge deflection increased. Finally, the main cables reached the ultimate capacity and ruptured, leading to the collapse of the entire bridge in cases PDI1 and PDI3. Before the collapse, the bridge had already experienced a large downward deflection, especially in the center span. In the case of PDI2, although the bridge did not collapse at the end of the simulation time, it had extremely large deflections in all three spans, which were significantly above the allowable values, and thus it was regarded that the ultimate state was reached.

Key LSs of the prototype suspension bridge

As the LL increased gradually, some structural members of the bridge started to fail, even though the entire bridge was still intact, and more members failed progressively. Finally, the entire bridge failed after reaching its ultimate state. All these member-failure events were recorded. Table 1 shows the events of first-member failures captured in the case of PDI1 by their occurrence sequences and the corresponding LL factors (LLFs). For each type of key structural component, only the first-member failure is presented. In total, 17 failure events are summarized. The first failure event

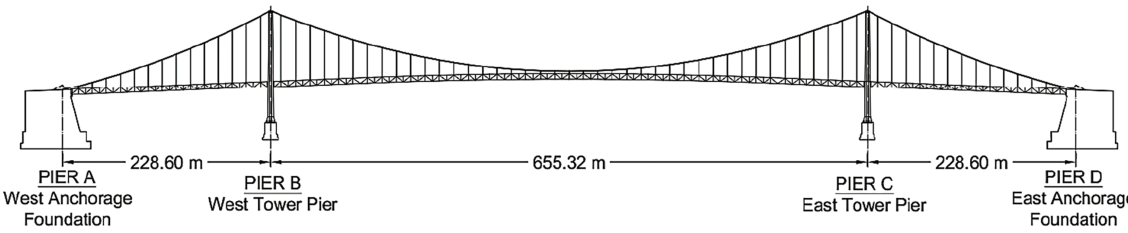

(a) Suspension Bridge

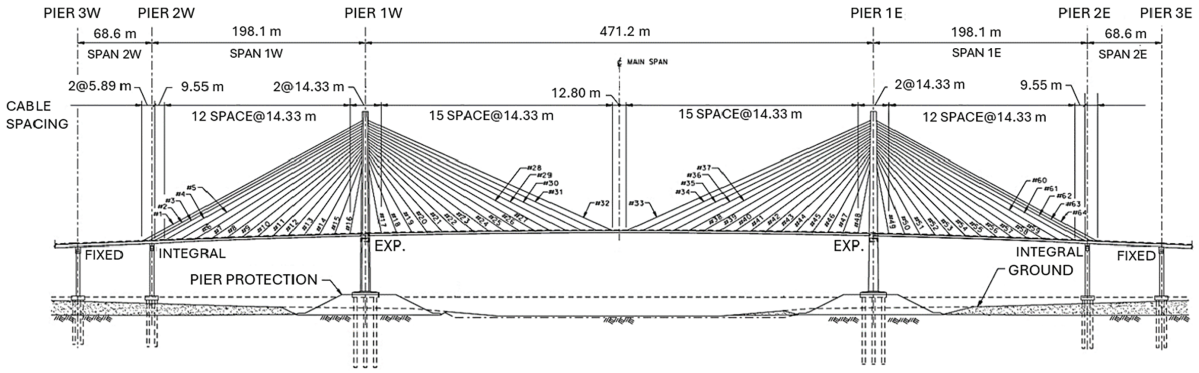

(b) Cable-stayed Bridge

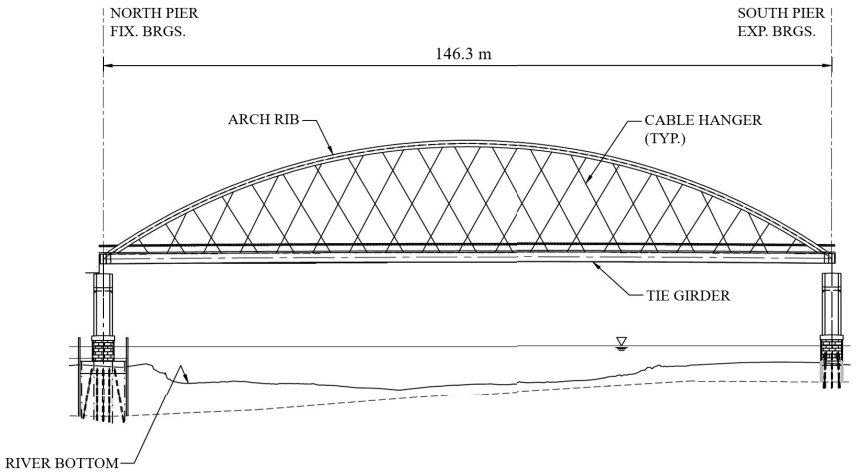

(c) Tie-arch Bridge

Figure 1. The prototype bridges

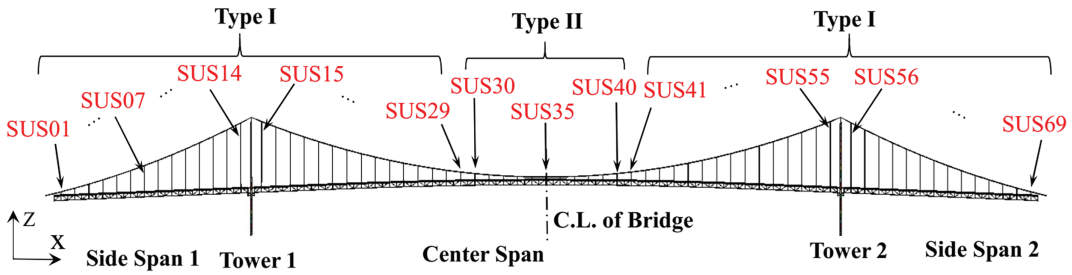

Figure 2. Suspender ID designation

is the sudden start of slipping of the main cable over a tower saddle, and the second one is the yield of a main cable. Similarly, these events were also observed in cases PDI2 and PDI3. Moreover, the global behavior of the bridge was significantly affected by them. In addition, although the yielding of a suspender in Table 1 occurred later than many other events, a suspender is a key structural component that is very vulnerable to loss. Thus, to evaluate the bridge performance for the intact and damaged states, three events in total are selected as the key LSs: (i) LS1—slipping of main

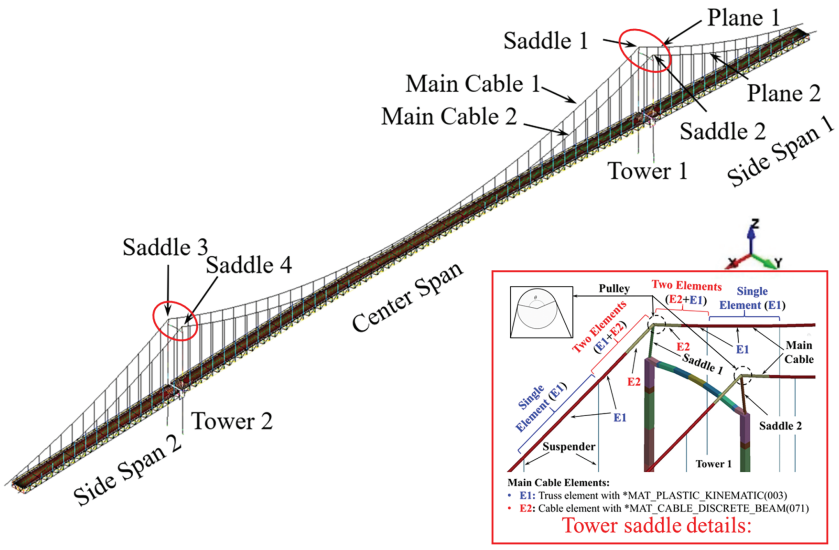

Figure 3. The FE model of the suspension bridge

cable over tower saddle; (ii) LS2—yielding of main cable; and (iii) LS3—yielding of suspender, which are summarized in Table 2.

Of all three LL cases, LS1 was reached in the case of PDI3 with a minimum LLF of 1.62. LS2 was reached in the case of PDI1 with a minimum LLF of 8.25, while it was not observed in the case of PDI2, since the main cables were still elastic at the end of the stimulation time. LS3 was reached in the case of PDI2 with a minimum LLF of 19.67.

Bridge deflection

The maximum deflections of the bridge (both downward and upward) during each push-down analysis are plotted against LLF in Fig. 4, with LS highlighted. In the case of PDI1, all three spans deflected downward, with the maximum deflection occurring at the center span. As represented by the blue solid line in Fig. 4a, the deflection pattern generally follows a "bilinear" trend divided into two "linear" phases around the second limit state (LS2). After the main cable yields, the deflection rate notably accelerates after LS2. In the case of PDI2, the side spans went downward, while the center span went upward. The maximum downward deflection in the center span and the maximum upward deflection in the side spans are plotted against LLF, as represented by the red dashed-and-dotted lines in Figs. 4a and 4b, respectively. Overall, the deflections increase with the increase of LLF until the end of the simulation, and this is more significant in the side spans. In the case of PDI3, the center span deflected downward, while the side spans went upward. The maximum downward deflection in the center span and the maximum upward deflection in the side spans are plotted against LLF, as represented by the black dashed lines in Figs. 4a and 4b, respectively. Similarly to the case of PDI1, the curve of downward deflection versus LLF exhibits an approximately "bilinear" trend, with two "linear" stages distinguished by LS2. Overall, the upward deflection in the side spans increases with the increase of LLF.

Slipping of the main cable

Under DL and LL, although the main cable forces at the two sides of the tower saddles were unbalanced, no slipping occurred because of the friction between the main cables and saddles. During push-down analyses, the unbalanced forces near the tower saddles kept increasing gradually as the LL increased. There was still no slipping at the initial stage with a lower LLF. However, slipping initiated suddenly once the unbalanced forces breached the friction threshold and led to unwanted deflections in the bridge deck. It occurred much earlier in cases PDI2 and PDI3 than in the case of PDI1, since the LL was applied on the side spans (case PDI2) or the center span (case PDI3) only, and the unbalanced forces increased more rapidly, especially in the case of PDI3. The slipping also led to readjustments in the geometrical configuration and tension of a main cable. Once the unbalanced cable force fell below the friction threshold, slipping stopped, and a rebalanced state was achieved in the main cable.

In all three cases, the first failure event is slipping of the main cable over the tower saddle. The slippages of Main Cable 1 over Saddle 1 or Saddle 3 are selected and plotted against LLF in Fig. 5. As shown in Fig. 5a, Main Cable 1 overall slipped three times in the case of PDI1, in spite of temporary rebalanced states during each time. It started to slip for the first time (i.e., LS1) at LLF = 4.44, and it continued to slip with the increase of the LL until the slippage reached 0.167 m at LLF = 8.29, which was slightly after LS2. Then, no further slipping occurred until the LLF reached 21.14. Afterward, the main cable slipped twice, and finally, the slippage reached 0.275 m when the main cable ruptured at LLF = 22.04. As shown in Fig. 5b, after LS1, the slippage in cases PDI2 and PDI3 increases monotonically with LLF, that is, the main cable continued to slip over the saddle until the end of the simulation. This is significantly different from the slipping in the case of PDI1, in which it occurred in spurts. Moreover, LS1 occurred much earlier in these two cases with lower LLF, that is, at LLF = 2.04 in the case of PDI2 and at LLF = 1.62 in the case of PDI3,

Table 1. Failure events for intact bridge during push-down analysis—Case PDI1

No.	Events	Deflection (m)	LLF
1	**Slip of main cable over tower saddle, start (first slip)**	2.176	4.44
2	**Yield of main cable**	4.497	8.25
3	Slip of main cable over tower saddle, end (first slip)	4.517	8.32
4	Buckling of diagonal member, side span	4.638	8.59
5	Yield of top chord (Type I)	12.384	11.53
6	Yield of bottom chord (Type II)	13.535	11.86
7	Yield of bottom chord (Type III)	13.634	11.89
8	Yield of bottom chord (Type I)	13.857	11.95
9	Buckling of diagonal member, main span	14.065	12.00
10	Buckling of tower link, main span	14.641	12.16
11	Yield of top chord (Type II)	15.447	12.39
12	Yield of tower link buckling (side span)	23.902	15.50
13	Yield of vertical member (Type II)	31.451	18.71
14	Slip of main cable over tower saddle, start (second slip)	37.662	21.14
15	Slip of main cable over tower saddle, end (second slip)	37.932	21.21
16	**Yield of suspender (Type I)**	38.973	21.94
17	Rupture of main cable	39.278	22.04

Table 2. Limit states from push-down analyses on intact bridge

No.	Limit states	LLF		
		PDI1	PDI2	PDI3
LS1	Slip of main cable over tower saddle	4.44	2.04	1.62
LS2	Yield of main cable	8.25	N.A.	8.73
LS3	Yield of suspender	21.94	19.67	21.84

respectively. The plot of slip versus LLF for the case of PDI2 follows approximately a "linear" trend. The slipping in the case of PDI3 increased more rapidly after the slippage reached 1.210 m with an LLF of 16.64. Finally, the slippages reached 4.091 m in the case of PDI2 and 3.847 m in the case of PDI3, respectively, which are around 14 times the slippage in the case of PDI1. Additionally, the slipping time histories of the main cables over the four saddles in the case of PDI3 are shown in Fig. 5c representatively. It is observed that the main cables started to slip simultaneously at t = 21.86 s, corresponding to an LLF of 1.62. Then, they continued to slip from the side spans to the center span until the end of the simulation.

Analysis results of damaged bridge with single-member loss

Following the simulation steps described for the intact bridge, push-down analyses of damaged bridges (PDD) were also conducted, that is, after they suffered single-suspender loss. Thirty-five single-suspender-loss scenarios were considered for the prototype suspension bridge. The 35 single-suspender-loss scenarios were loss of SUS.01 to SUS.35, as shown in Fig. 2. All 35 single-suspender-loss scenarios were investigated for the three live-load distribution patterns LL1 to LL3. In this study, only single-suspender-loss cases were investigated. Correspondingly, they are divided into three groups, which are denoted by PDD1, PDD2, and PDD3, respectively. The three key LSs (i.e., LS1–LS3) were also evaluated during the push-down analyses of the damaged bridges.

The LLFs of PDD1 are shown in Fig. 6a. For LS1 (slip of main cable over tower saddle), the LLFs are in a narrow range of 4.35–4.45, and the relative differences are less than 2.0% in comparison with the LLF of LS1 in the case of PDI1. The load factors of PDD1 for LS2 (yield of main cable) show only slight deviations up to 1.5% from the LLF of LS2 in the case of PDI1. Notably, LS3 (yield of suspender) displays a significant drop in LLFs in most damaged cases of PDD1, except for the case SR35 (removal of suspender No. 35), the LLFs of all other damaged bridges are lower than that of the intact bridge (case PDI1), and the relative differences

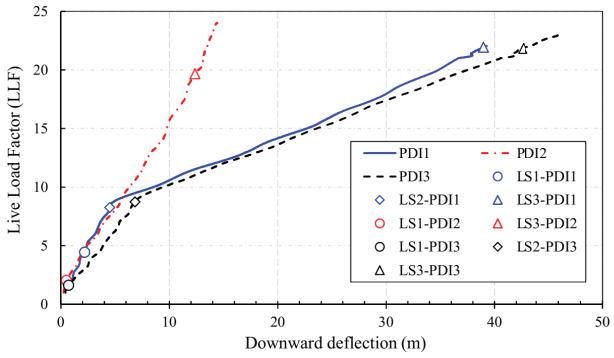

(a) LLF vs. Downward deflection

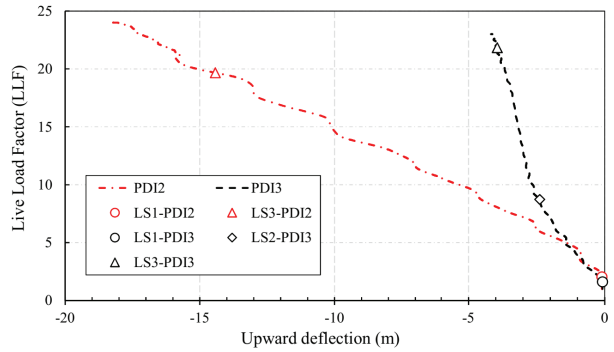

(b) LLF vs. Upward deflection

Figure 4. Limit states for intact bridge during push-down analyses

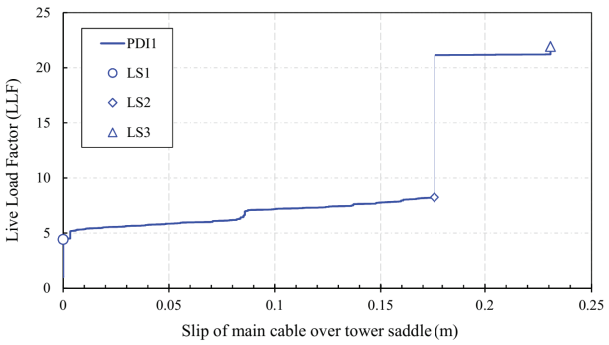

(a) Slipping over Saddle 3 in PDAI1

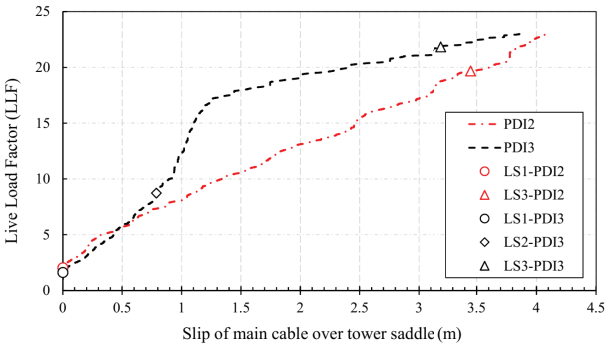

(b) Slipping over Saddle 1 in PDAI2 & PDAI3

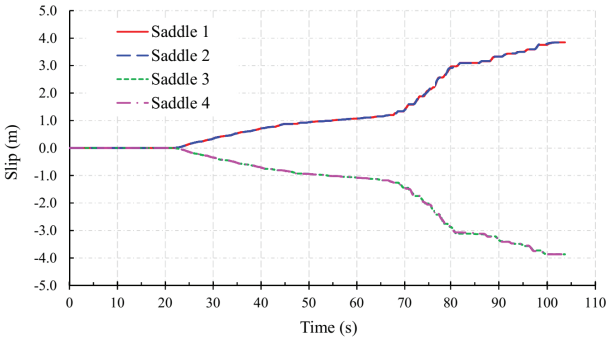

(c) Slipping time history of main cables in PDAI3

Figure 5. Slip of main cables during push-down analyses of intact bridge

with respect to that of the intact bridge are in the range of −41.2% to −12.5%. For each damaged bridge case, the suspenders adjacent to the removed suspender dominate LS3. Thus, for cases SR01–SR30, the LLFs are dominated by the Type I suspenders (i.e., SUS02–SUS29) and for cases SR31–SR35, the LLFs are dominated by the Type II suspenders (i.e., SUS30–SUS34). Since Type II suspenders have a larger cross-section, the LLFs of cases SR31–SR34 increase by approximately 3.0 with respect to those of cases SR24–SR30. Due to the support provided by towers, the influence of single-suspender loss on LLFs close to towers is found to be less significant. Thus, the LLFs of SR14 and SR15 are larger than the LLFs of other cases nearby. Additionally, from SR08 to SR14, the LLF increases gradually, whereas the LLF decreases gradually from SR15 to SR27.

The LLFs of PDD2 are shown in Fig. 6b. For LS1 (slip of main cable over tower saddle), it was slightly affected when the SSR occurred in the side span, and the relative differences are less than 2.3%. However, for an SSR in the center span, LS1 may be affected significantly. Overall, the LLFs of cases SR15–SR35 are less than that of the intact bridge, and the maximum relative difference is 19.0%. The minimum LLF is 1.65, which occurred in the case of SR28. Similarly in the case of PDI2, LS2 (yield of main cable) was not reached in the group of PDD2. The influence of SSR on LS3 (yield of suspender) is mainly observed in side spans where the LLs were applied. The LLFs of the damaged bridges for cases SR01–SR14 are all less than that of the intact bridge (case PDI2). The minimum LLF is 13.70, which occurred in the case of SR08 with a relative difference of −30.4%. Similar influence is also found in the center span, but limited to cases SR15 and SR16, in which SRs were very close to Tower 1. The LLFs of other SSR scenarios in the center span (i.e., cases SR17–SR15) are very close to the LLF of PDI2, and the maximum difference is −1.8%.

The LLFs of PDD3 are shown in Fig. 6c. For LS1 (slip of main cable over tower saddle), the LLFs are in a narrow range of 1.58–1.64, and the relative differences are less than 2.7% in comparison with the LLF of LS1 in the case of PDI3. For LS2 (yield of main cable), the LLFs are in a narrow range of 8.71–8.74, and the relative differences are less than 0.2% in comparison with the LLF of LS2 in the case of PDI3. The effect of SSR on LS3 (yield of suspender) varies significantly with the location of suspender loss. Specifically, only a slight effect is observed when the SR occurs in side spans (e.g., cases SR01–SR12), while a significant effect is observed when it occurred in the center span. However, for cases SR13 and SR14, although the suspender loss occurred in Side Span 1, the influence increases because of their location close to

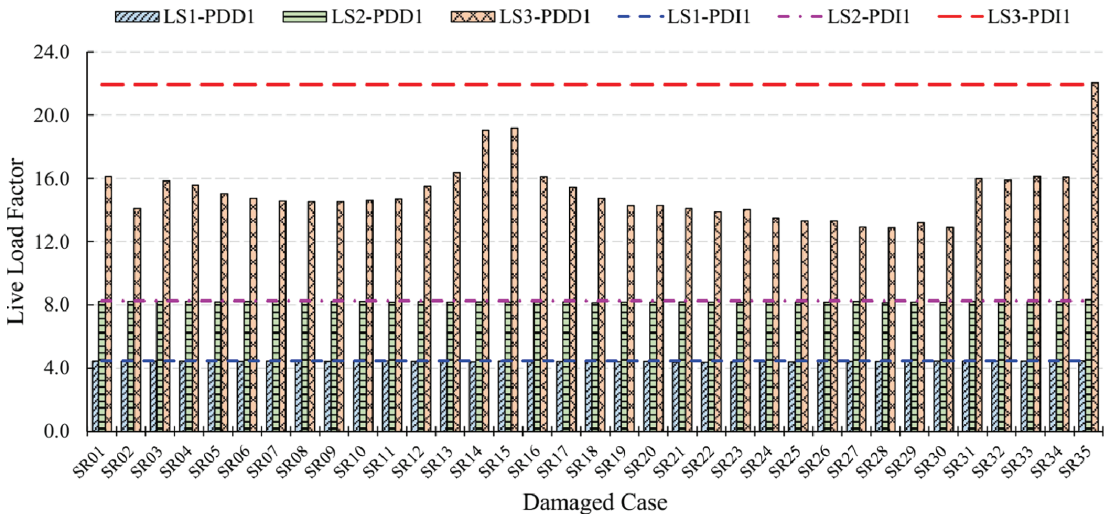

(a) Load factors of PDD1

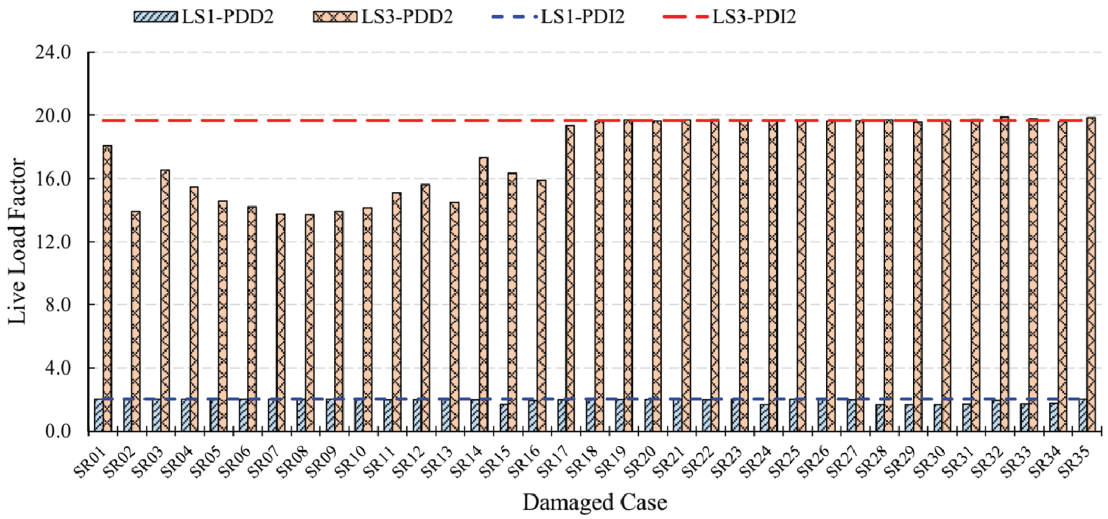

(b) Load factors of PDD2

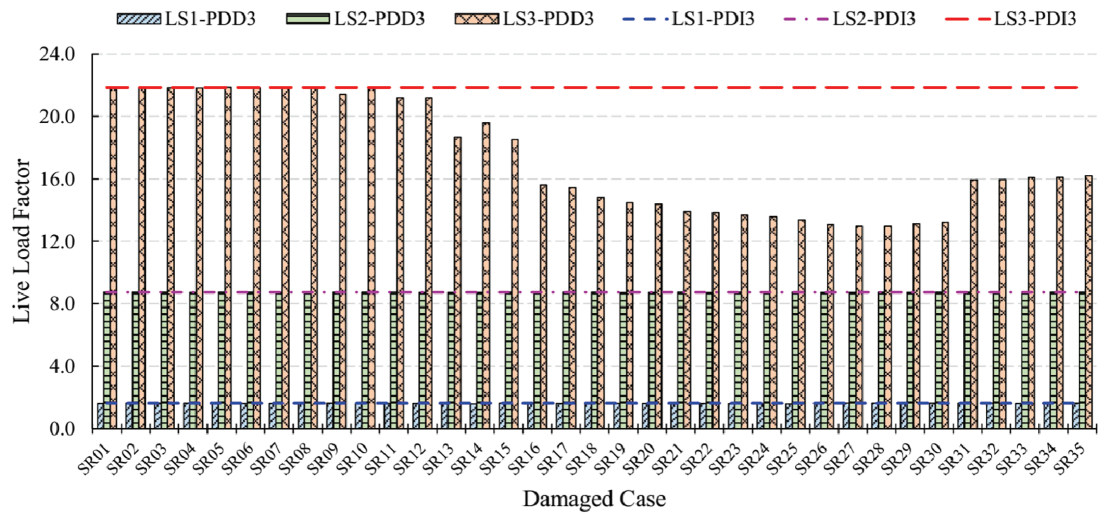

(c) Load factors of PDD3

Figure 6. Load factors of push-down analysis of damaged bridge (suspension bridge)

Tower 1, and the LLF drops to around 19.0 from a value of 21.84 for the intact bridge. A more noticeable effect of suspender loss on LS3 is observed in the center span. From SR15 to SR30, the LLF decreases monotonically at first and then fluctuates slightly around 13.0. The minimum is 12.96, which occurred in the case of SR27 with a relative difference

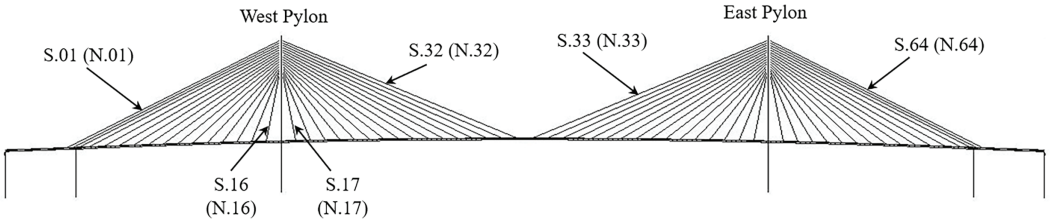

Figure 7. Cable ID designation in the cable-stayed bridge

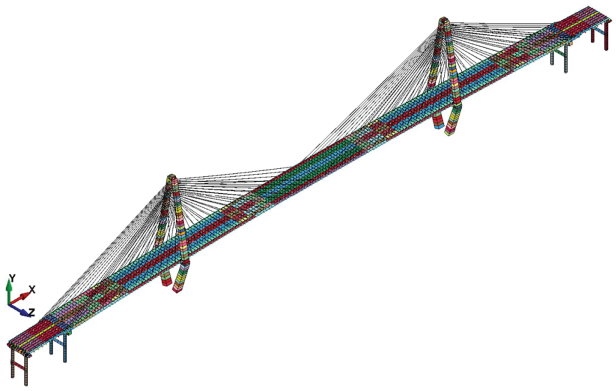

Figure 8. The FE model of the prototype cable-stayed bridge

of −40.6%. The declining trend terminates at case SR30. Afterward, the LLF increases abruptly and stays around 16.0 for cases SR31–SR35, since Type II suspenders start to dominate LS3 from case SR31.

Cable-Stayed Bridge

As shown in Fig. 1b, a cable-stayed bridge was selected as the second prototype bridge. It consists of a 471.2-m center span, two 98.1-m side spans, and two 68.6-m approach side spans. Two longitudinal steel edge girders continue over the center span and two side spans, and they are supported by 64 pairs of cables in a semi-fan arrangement, with a cable spacing of 14.33 m at the deck level, except for the four backstays near each anchor pier. The bridge is 42.7 m wide, accommodating eight traffic lanes and one walkway on the south side. The diamond-shaped concrete pylons are 175.0 m high. The cable IDs (Fig. 7) increase from left (west side) to right (east side). Here, "S (or N)" represents South Plane (or North Plane). The FE model of the cable-stayed bridge developed in LS-DYNA® is shown in Fig. 8. The details about the model's construction, calibration and validation, material nonlinearity consideration, load application, and member removal simulation process can be found in Chen et al.[20].

Three LL distributions were presented in this paper as follows: (1) LL1—uniform LL was applied on all five spans; (2) LL2—uniform LL was applied on the two side spans only; and (3) LL3—uniform LL was applied on the center span only.

Analysis results of intact bridge

Push-down analyses were first conducted on the intact bridge under the three live-load distributions, that is, LL1–LL3, and they are denoted by PDI1, PDI2, and PDI3, respectively. As the LL increased, the forces increased in the major structural components of the cable-stayed bridge, which include the bridge pylons, stay cables, and main girder members. Finally, the stay cables reached the ultimate capacity and ruptured, leading to the collapse of the entire bridge in cases PDI1 and PDI2. In the case of PDI3, due to large, unbalanced loads between the center span and side spans during push-down analysis when the applied LL at the center span increased, the bridge pylon failed, leading to the collapse of the entire bridge.

Key LSs of the prototype cable-stayed bridge

The maximum vertical downward displacement of the bridge deck with respect to the LLFs for case PDI1 is illustrated by the solid blue line in Fig. 9. In the case of PDI1 of the cable-stayed bridge, the first cable (Cable S.22) reached its yield strength at an LLF of 7.95, which is the first-member failure and marked by a circle along the solid blue line. The rate of displacement at the deck level remained steady after the first cable yielded. As the LL continued to increase, more cables yielded, causing the main girder to become highly stressed as it lost support from the cables. When the first girder member yielded at an LLF of 8.92, marked by a diamond along the blue solid line, the maximum vertical displacement suddenly increased, as reflected by the reduced slope of the curve. At this point, 46 out of 128 cables had reached their yield strength. As the LL further increased, more cables and girder members yielded, leading to a significant decrease in bridge stiffness. The lateral bearing connecting the bridge pylon and girder failed when the LLF reached 9.74. At this stage, 80 out of 128 cables had reached their yield strength. The first cable (Cable S.22) ruptured when the LLF reached 9.89 just after failure of the lateral bearing, marked by a triangle along the solid blue line. With a further small increase in the LLF, many more cables reached their ultimate strength and ruptured, leading to the collapse of the whole bridge.

The maximum vertical downward displacement of the bridge deck with respect to the LLFs for case PDI2 is illustrated by the red dashed-and-dotted line in Fig. 9. In the case of PDI2 of cable-stayed bridge, the first main girder member reached its yield strength first at an LLF of 3.59, marked by a diamond along the red dashed-and-dotted line. The rate of displacement at the deck level remained steady after the first girder member yielded. As the LL continued to increase, the

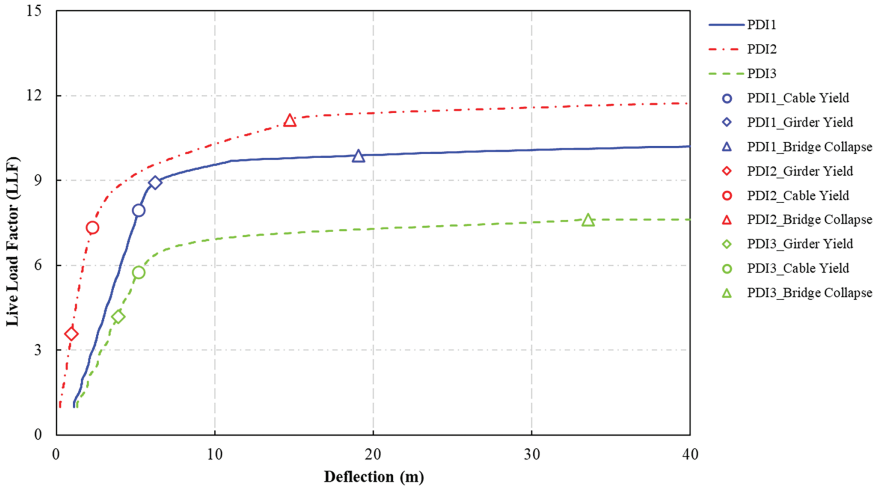

Figure 9. Load–displacement curve of push-down analysis of intact bridge (cable-stayed bridge)

Table 3. Limit states from push-down analyses on intact bridge (cable-stayed bridge)

No.	Limit states	LLF		
		PDI1	PDI2	PDI3
LS1	Yield of main girder	8.92	**3.59**	**4.18**
LS2	Yield of stay cable	**7.95**	7.35	5.75
LS3	Bridge collapse	9.89	11.14	7.63

first cable yielded at an LLF of 7.35, marked by a circle along the red dashed-and-dotted line, and the maximum vertical displacement also suddenly increased after reaching this limit state. As the LL was further increased, more cables and girder members yielded, leading to a significant decrease in the bridge stiffness. The first cable (Cable ID S.12) ruptured (the third limit state) when the LLF reached 11.14, marked by a triangle along the red dashed-and-dotted line. With a further small increase in the LLF, many more cables reached their ultimate strength and ruptured, leading to the collapse of the whole bridge.

The maximum vertical downward displacement of the bridge deck with respect to the LLFs for case PDI3 is illustrated by the green dashed line in Fig. 9. In the case of PDI3 of cable-stayed bridge, the first main girder member reached its yield strength first at an LLF of 4.18, marked by a circle along the green dashed line. The rate of displacement at the deck level remained steady after the first girder member yielded. As the LL continued to increase, the first cable LS would yield at an LLF of 5.75, the maximum vertical displacement suddenly increased after the first cable yield, as reflected by the reduced slope of the curve. As the LL was further increased, more cables and girder members yielded, leading to a significant decrease in the bridge stiffness. The lateral bearing connecting the bridge pylon and girder failed when the LLF reached 7.41. At this stage, 24 out of 128 cables had reached their yield strength. As the LL continued to increase, the center span and the side span were subjected to large, unbalanced loads, and the bridge pylons were under large bending moments. The bridge pylons failed when the LLF reached 7.63 just after failure of the lateral bearing. With a further small increase in the LLF, many more cables reached their ultimate strength, leading to the collapse of the whole bridge.

Although the failure modes and sequences differ among the three cases due to different LL configurations, they exhibit some common characteristics. The load-displacement curves indicate that the bridge behaves elastically with stable deflection until the first-member failure occurs, as shown by the initial steep slopes of the curves. As the LL increases further, a slight decrease in the bridge's stiffness is observed, reflected by the changing slopes of the curves. With continued increments in LL, a more significant reduction in stiffness occurs, indicated by the flattening of the curves, and the bridge eventually reaches its ultimate capacity and collapses. Three key LSs were identified for all three push-down cases, as summarized in Table 3. Of all three push-down cases, LS1 (yield of main girder member) was first reached in the case PDI2 with the lowest LLF of 3.59, followed by an LLF of 4.18 in PDI3. In contrast, in the case of PDI1, LS1 occurred after LS2 (yield of stay cable), indicating that the main girder member is more vulnerable under an unbalanced LL configuration between the side span and center span. LS1 (yield of stay cable) was first reached in the case of PDI3 with the lowest LLF of 5.75, followed by an LLF of 7.35 in PDI2 and an

LLF of 7.95 in PDI1. LS3 (bridge collapse) was first reached in the case of PDI3 with the lowest LLF of 7.63, followed by an LLF of 9.89 in PDI1. In contrast, the LLF for LS3 in PDI2 is slightly more distant from LS2 compared to the other cases. This is because the LL is applied only to the side span, which is relatively shorter, requiring a larger LLF to cause the collapse of the entire bridge.

Analysis results of damaged bridge with single-member loss

Following the simulation steps described for the intact bridge, push-down analyses were also conducted on damaged bridges, that is, after they suffered single stay-cable loss. A total of 32 single-cable-loss scenarios were considered for the prototype cable-stayed bridge, corresponding to the loss of Cables S.01–S.32, as shown in Fig. 7. All 32 cable-loss scenarios were investigated for the three live-load distribution patterns LL1–LL3. Correspondingly, they are divided into three groups, which are denoted by PDD1, PDD2, and PDD3, respectively. The three LSs (i.e., LS1–LS3) were also evaluated during the push-down analyses of the damaged bridges.

The LLFs of PDD1 are shown in Fig. 10a. The loss of the long cables at the side span (Cables S.01–S.06) had a relatively smaller effect on the LLF for the first cable yield, first girder member yield, and ultimate collapse LSs, since these cables were near the support provided by the auxiliary pier and their spacing is relatively small compared to other cables. The loss of the cables near the bridge pylon (Cables S.15–S.18) had a relatively small effect on the first cable yield and ultimate collapse LSs, because the cable forces in these cables were relatively smaller than in the other cables and the bridge ultimate collapse initiated by cable rupture in PDD1. However, the loss of the cables near the bridge pylon (Cables S.15–S.18) had a relatively large effect on the first girder yield limit state, because the girder members near the bridge pylon were under large compression force. The girder member yields prior to first stay-cable yield in PDD1 with loss of the cables near the bridge pylon (Cables S.15–S.18). The loss of cables at the center of the side span and middle span caused a larger drop in the LLF for all three LSs. Loss of Cable S.10 in the side span and loss of Cables S.23–S.25 in the center span were the most critical cases with the lowest LLFs for the first cable yield and ultimate collapse LSs; loss of Cables S.31 and S.32 were the two most critical cases for the first girder member yield limit state.

The LLFs of PDD2 are shown in Fig. 10b. The LLFs corresponding to all the three LSs show a similar trend. Since the LL was applied only on the side span, the cables at the side span played a significant role during the push-down analysis. The loss of cables at the center of the side span (S.05–S.10) and middle span (S.30–S.32) caused a larger drop in the LLF for the first girder LSs. The loss of other cables had a relatively smaller effect on the LLF for the girder yield limit state. The loss of cables at the center of the side span (S.07–S.14) had a relatively larger effect on the cable yield limit state, and the loss of cables at the center of the side span (S.07–S.16) had a relatively larger effect on the ultimate collapse limit state. Overall, loss of Cable S.10 in the side span was the most critical case with the lowest LLFs for the first cable yield LS and ultimate collapse LS.

The LLFs of PDD3 are shown in Fig. 10c. Since the LL was applied only on the center span, there were large, unbalanced loads between the center span and side spans during push-down analysis when the applied LL at the center span increased. Hence, the cables at the side span played a significant role against the unbalanced load at the center span, especially the longest cables at the side span (Cable IDs S.01–S.04). In all LSs, the first girder yield, first cable yield, and ultimate collapse LSs, the loss of the longest cables at the side span (Cable IDs S.01–S.04) had a relatively larger effect on the LLF. The loss of the longest cables at the center span (Cable IDs S.28–S.32) also had a relatively larger effect on these LSs, because the cable forces in these cables were relatively larger than in the other cables. The loss of other cables had a relatively smaller effect on the LLF for these three LSs. Overall, loss of Cable IDs S.01 and S.02 in the side span were the most critical cases with the lowest LLFs for all the LSs.

Tied-Arch Bridge

As shown in Fig. 1c, a single-span tied-arch bridge was selected as the last prototype bridge. The bridge is 146.30 m long and 30.58 m wide, accommodating four traffic lanes and a shared path for pedestrians and bicycles on the south side. The two steel main arches are 23.16 m high, and they are connected transversely with eight X-shaped top bracings and two transverse beams. The two tie girders are supported by 36 pairs of hangers in a network arrangement from the arches. The hanger spacing is 3.66 m at the girder level (i.e., anchor points). The hanger ID information is shown in Fig. 11. The hanger IDs increase from left (north side) to right (south side). Here, "W (or E)" represents West Plane (or East Plane). A three-dimensional FE model of the bridge was also developed in LS-DYNA®, as shown in Fig. 12. HL-93 design LL, which consists of a combination of the design truck and lane load, was applied on the bridge as per AASHTO LRFD.[21] The details about the model's construction, calibration and validation, material nonlinearity consideration, LL application, and member removal simulation process can be found in Chen et al.[22].

Analysis results of intact bridge

Like the other two prototype bridges, push-down analysis was first conducted on the intact bridge under the design LL. With the increasing LL, the bridge deflection increased, and three LSs were identified. The LLF versus the maximum vertical deflection of the deck during push-down analysis is shown in Fig. 13. The first hanger to reach its yield strength, at an LLF of 11.95, was W.03. As the LL was further increased, more hangers yielded, and eventually the

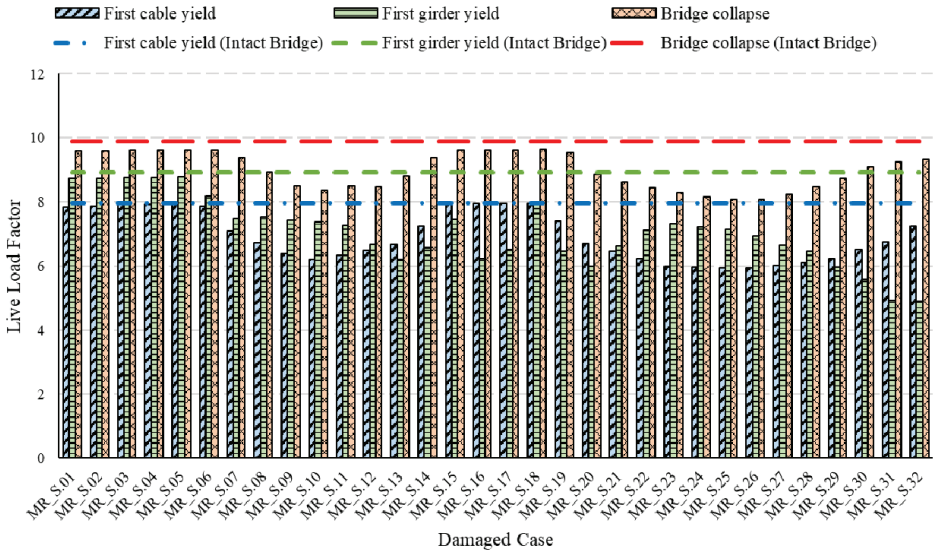

a) Load factor of PDD1

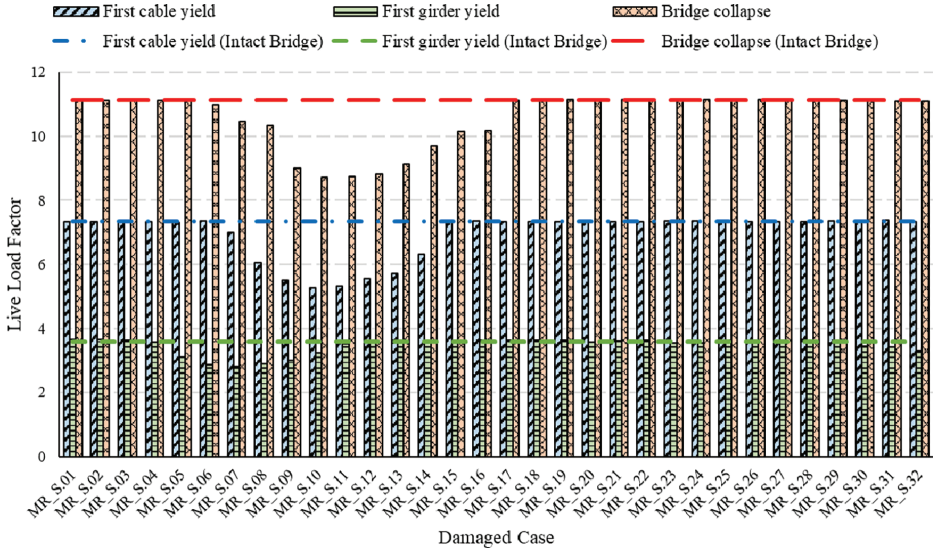

b) Load factor of PDD2

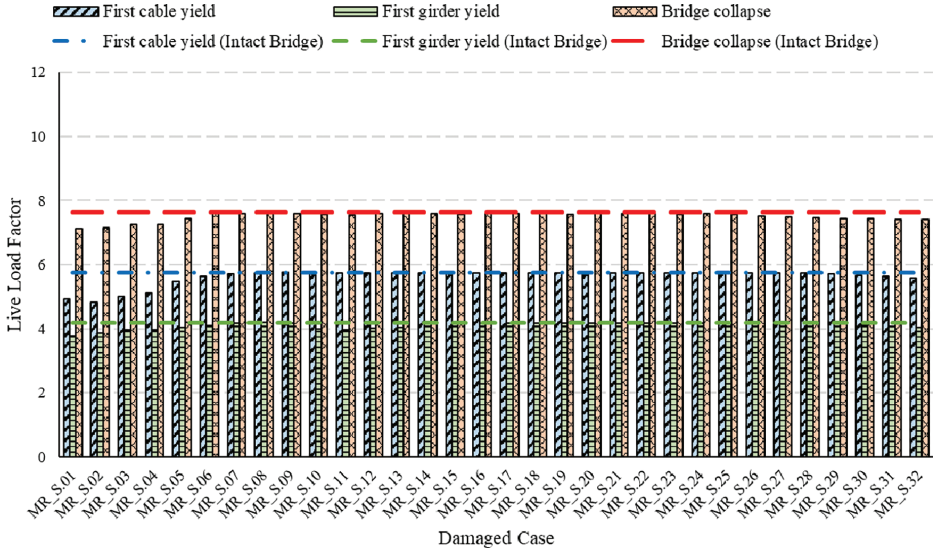

c) Load factor of PDD3

Figure 10. Load factors of push-down analysis of damaged bridge (cable-stayed bridge)

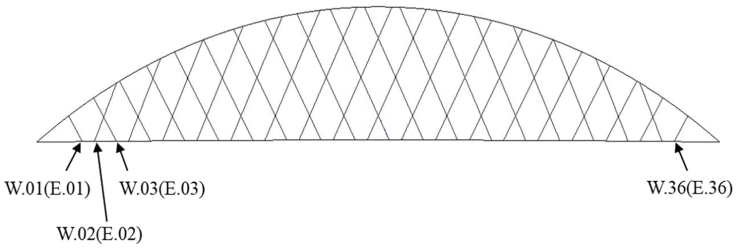

Figure 11. Hanger ID designation in the tied-arch bridge

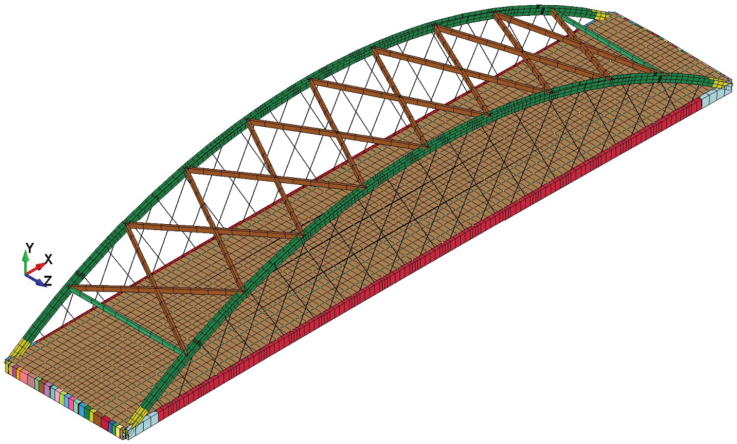

Figure 12. The FE model of the prototype-arch bridge

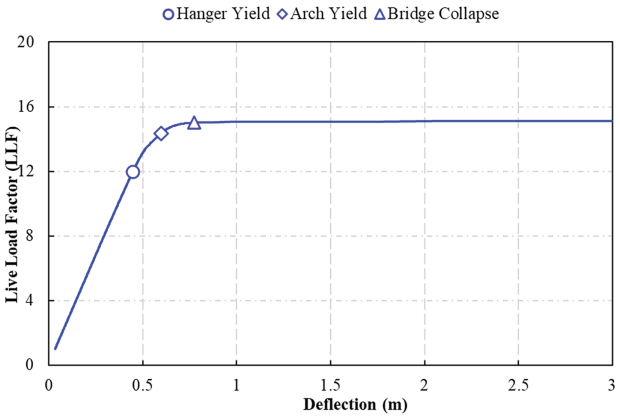

Figure 13. Load–displacement curve of push-down analysis of intact bridge (arch bridge)

maximum vertical displacement increased suddenly as the LLF reached 14.35. This corresponded to the second limit state: arch member yield. As the LL further increased, more hangers yielded, and the yield zone in the arch spread, causing the stiffness of the bridge to decrease significantly. Eventually, the third LS was reached, that is, hanger rupture. This occurred at W.03 at an LLF of 15.01. With a small increase in the LLF at this point, many more hangers reached their ultimate strength and ruptured, leading to the collapse of the entire bridge. The girder members only reached their yield strength and ultimate strength after the bridge started to collapse.

Analysis results of damaged bridge with single-member loss

Following the simulation steps described for the intact bridge, push-down analyses were also conducted on damaged bridges that experienced a single hanger-loss event. Eighteen single-hanger loss scenarios were considered for the prototype tied-arch bridge, corresponding to the loss of hangers W.01–W.18, as shown in Fig. 11. The load factors for the damaged bridge at the three LSs, the first hanger yield (blue bars with diagonally hatched pattern), first arch yield (green bars with horizontally hatched pattern), and bridge collapse (yellow bars with cross-hatched pattern), as identified earlier during the push-down analysis, are presented in Fig. 14.

Similar to the intact bridge, the damaged bridge exhibits a consistent trend across different hanger-loss scenarios. The first hanger yields at a lower LLF, followed by the yield of the arch member, and ultimately leading to the collapse of the bridge. In the push-down analysis of the damaged bridge, the simulations showed that the arch moved upward at the hanger-loss location and eventually buckled due to the combined effect of compressive force and biaxial bending moment in the arch. As a result, the hangers adjacent to the lost hanger reached their ultimate strength and eventually ruptured, leading to the collapse of the entire bridge.

The loss of hangers slanted backwards, such as W.01, W.03, and W.05, had a lower LLF than the loss of hangers slanted forward. Additionally, the loss of hangers near the center span of the bridge was found to be less critical than

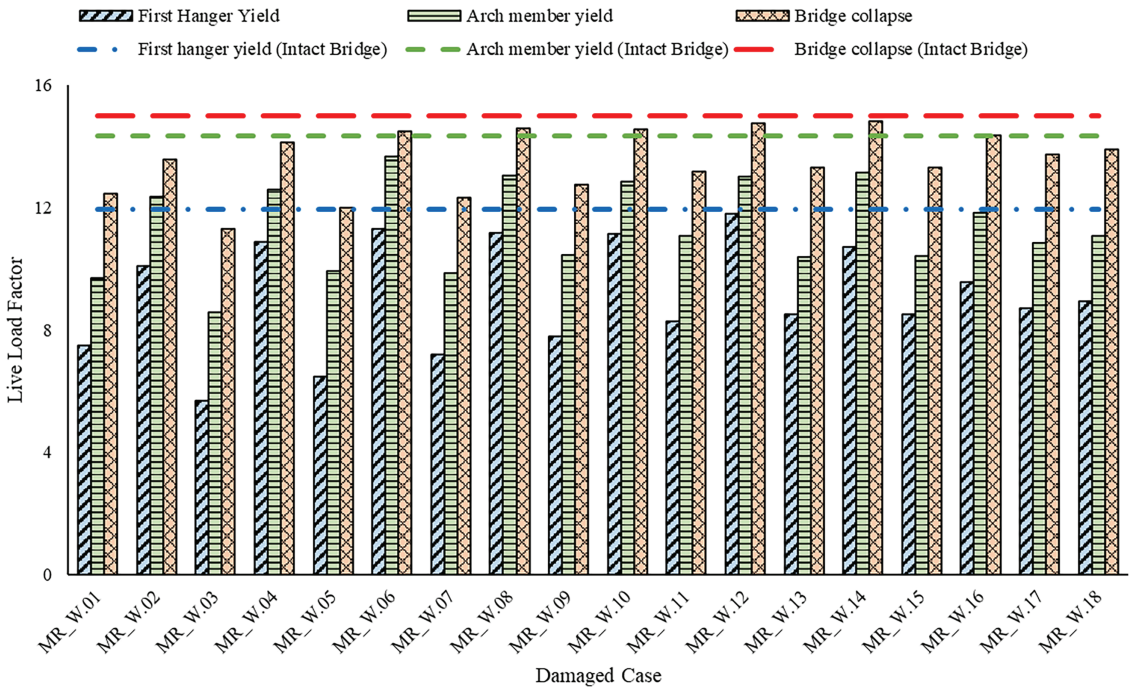

Figure 14. Load factors of push-down analysis of damaged bridge (arch bridge)

the loss of hangers in the end zones. Among all the hanger-loss scenarios, the loss of hanger W.03 was the most critical case with the lowest LLF corresponding to all the three LSs.

Conclusions

In this paper, the key LSs for structural robustness evaluation of three prototype long-span cable-supported bridges were investigated through push-down analyses for both the intact states and the damaged states due to single cable loss. The main conclusions are summarized as follows:

For each example bridge, push-down analysis was conducted on the intact bridge under the selected live-load distributions. Based on the analysis of the three bridges, they exhibited similar overall behavior during the push-down analysis. Initially, they showed a near-linear elastic response, where the structures deformed proportionally to the load without any permanent damage. This stage was followed by a progressive stiffness degradation as critical components yielded and load redistribution occurred. Ultimately, each bridge reached its capacity and collapsed eventually. Key structural components of the bridge were monitored closely during the push-down process, such as main cables, suspenders/stay cables/hangers, main girders, main arches, and so on. Based on the bridge behavior during push-down analysis, three key LSs were identified for each bridge, each LS reflecting a distinct change in structural behavior. The first key LS corresponds to the initial member failure, marking the point where a structural component first yields and the bridge exceeds its design requirements. The second LS indicates major stiffness degradation, where small load increments result in large deflections. The third key LS represents ultimate collapse, where the bridge can no longer sustain any additional load.

For the suspension bridge, three key LSs were identified: (1) slip of main cable over tower saddle, (2) main cable yield, and (3) suspender yield. For the cable-stayed bridge, three key LSs were identified: (1) stay-cable yield, (2) main girder yield, and (3) stay-cable rupture. For the tied-arch bridge, three LSs were identified: (1) hanger yield, (2) main arch yield, and (3) hanger rupture. The LLF corresponding to each LS was recorded as the index to evaluate the LS quantitatively. It should be noted that the key LSs are also strongly influenced by the live-load configuration of the bridge and the design safety factors of individual components. For example, suspender yielding occurs last in the failure sequence during the push-down analysis, primarily because suspenders are designed with a large safety factor compared to other components and the applied LL configuration in the suspension bridge was distributed over a large portion of the spans.

The key LSs identified from the intact bridges were also investigated during the push-down analyses on the damaged bridges induced by single-cable loss, and the corresponding LLFs were compared with the LLFs of the intact bridges. The results showed that: (1) all three bridges have very high capacity for the design LLs, (2) the overall performances of the bridges were affected negatively by cable loss, and the effects varied with the location of cable loss and live-load distribution patterns, and (3) even with such adverse effects, the capacities of the damaged bridges were not reduced significantly.

Acknowledegments

This material is based upon work supported by the Federal Highway Administration under contract number DTFH61-14-D-00010/693JJ318F000170. Any opinions, findings, conclusions, or recommendations expressed in this publication are those of the author(s) and do not necessarily reflect the views of the Federal Highway Administration.

Data Availability Statement

All the data, models, or code that support the findings of this study are available from the corresponding author upon reasonable request.

References

[1] Kawai Y, Siringoringo D, Fujino Y. Failure analysis of the hanger clamps of the Kutai-Kartanegara Bridge from the fracture mechanics viewpoint. *J JSCE*. 2014;2(1):1–6. doi:10.2208/journalofjsce.2.1_1.

[2] Morgese M, Ansari F, Domaneschi M, Cimellaro GP. Post-collapse analysis of Morandi's Polcevera viaduct in Genoa Italy. *J Civ Struct Health Monit*. 2020;10(1):69–85. doi:10.1007/s13349-019-00370-7.

[3] TTSB. *Final Report on Nanfangao Sea-Crossing Bridge Collapse*. Report no. TTSB-HOR-20-11-001. Taiwan: Taiwan Transportation Safety Board; 2020.

[4] Frangopol DM, Curley JP. Effects of damage and redundancy on structural reliability. *J Struct Eng*. 1987;13(7):1533–1549. doi:10.1061/(asce)0733-9445(1987)113:7(1533).

[5] Ghosn M, Moses F. *Redundancy in highway bridge superstructures*. NCHRP Report No. 406. Washington, D.C: Transportation Research Board; 1998.

[6] Liu WD, Neuenhoffer A, Ghosn M, Moses F. *Redundancy in highway bridge substructures*. NCHRP Report No. 776. Washington, D.C: Transportation Research Board; 2001.

[7] Ghosn M, Yang J, Beal D, Sivakumar B. Bridge system safety and redundancy. In: *NCHRP Report No. 776*. Washington, D.C: Transportation Research Board; 2014.

[8] Maes MA, Fritzsons KE, Glowienka S. Structural robustness in the light of risk and consequence analysis. *Struct Eng Inter*. 2006;16(2):101–107. doi:10.2749/101686606777962468.

[9] Wisniewski D, Casas JR, Ghosn M. Load capacity evaluation of existing railway bridges based on robustness quantification. *Struct Eng Int*. 2006;16(2):161–166.

[10] Izzuddin BA, Vlassis AG, Elghazouli AY, Nethercot DA. Progressive collapse of multi-story buildings due to sudden column loss—Part I: simplified assessment framework. *Eng Struct*. 2008;30(5):1308–1318. doi:10.1016/j.engstruct.2007.07.011.

[11] Khandelwal K, El-Tawil S. Push down resistance as a measure of robustness in progressive collapse analysis. *Eng Struct*. 2011;33(9):2653–2661. doi:10.1016/j.engstruct.2011.05.013.

[12] Shoghijavan M, Starossek U. Structural robustness of long-span cable-supported bridges in a cable-loss scenario. *J Bridge Eng*. 2018;23(2):04017133. doi:10.1061/(asce)be.1943-5592.0001186.

[13] Chen Q, Wang H, Bhattacharya B, El-Tawil S, Agrawal AK, Wong W. Reliability-based framework for structural robustness evaluation of bridges. *J Bridge Eng*. 2024b;29(6):04024035.

[14] LSTC (Livermore Software Technology Corporation). LS-DYNA® keywords user manual volume II-material models; 2020. https://www.dynasupport.com/manuals/ls-dyna-manuals/ls-dyna_manual_volume_i_r12.pdf.

[15] Agrawal AK, El-Tawil S, Chen Q, Wang H. *Redundancy in Long Span Bridges for Risk Mitigation in a Multi-Hazard Environment*. United States: Federal Highway Administration; 2022.

[16] PTI (Post-Tensioning Institute). *Recommendations for Stay Cable Design, Testing and Installation*. 4th ed. Phoenix, AZ: Post-Tensioning Institute; 2007.

[17] AASHO. *Standard Specifications for Highway Bridges*. Washington, DC: AASHO; 1961.

[18] Wang H, Chen Q, Agrawal AK, El-Tawil S, Bhattacharya B, Wong W. Dynamic response and progressive collapse of a long-span suspension bridge induced by suspender loss. *J Struct Eng*. 2022;148(6):05022001. doi:10.1061/(asce)st.1943-541x.0003367.

[19] Wang H, Chen Q, Agrawal AK, El-Tawil S, Bhattacharya B, Wong W. Performance of a long-span suspension bridge subjected to sudden single suspender loss. *J Bridge Eng*. 2023;28(11):05023006. doi:10.1061/jbenf2.beeng-6108.

[20] Chen Q, Wang H, El-Tawil S, Agrawal AK, Bhattacharya B, Wong W. Progressive collapse behavior of a long-span cable stayed bridge induced by cable loss. *J Bridge Eng*. 2023;28(9):05023005. doi:10.1061/jbenf2.beeng-5840.

[21] AASHTO. *AASHTO LRFD Bridge Design Specifications*. 9th ed. Washington, D.C: American Association of State Highway and Transportation Officials; 2020.

[22] Chen Q, Wang H, El-Tawil S, Agrawal AK, Bhattacharya B, Wong W. Behavior of a network tied-arch bridge subjected to sudden hanger loss scenarios. *J Bridge Eng*. 2024a;29(1):05023010. doi:10.1061/jbenf2.beeng-6328.